



Strain rate dependence of twinning avalanches at high speed impact

L. Zhang, E. K. H. Salje, X. Ding, and J. Sun

Citation: [Applied Physics Letters](#) **104**, 162906 (2014); doi: 10.1063/1.4873520

View online: <http://dx.doi.org/10.1063/1.4873520>

View Table of Contents: <http://scitation.aip.org/content/aip/journal/apl/104/16?ver=pdfcov>

Published by the [AIP Publishing](#)

Articles you may be interested in

[Grain boundary orientation effects on deformation of Ta bicrystal nanopillars under high strain-rate compression](#)

J. Appl. Phys. **115**, 053528 (2014); 10.1063/1.4864427

[Growth of deformation twins in tantalum via coherent twin boundary migration](#)

J. Appl. Phys. **114**, 113511 (2013); 10.1063/1.4821956

[Hypervelocity impact induced deformation modes in \$\alpha\$ -alumina](#)

Appl. Phys. Lett. **91**, 071906 (2007); 10.1063/1.2753092


[Deforming nanocrystalline nickel at ultrahigh strain rates](#)

Appl. Phys. Lett. **88**, 061917 (2006); 10.1063/1.2173257

[Deformation twinning in nanocrystalline copper at room temperature and low strain rate](#)


Appl. Phys. Lett. **84**, 592 (2004); 10.1063/1.1644051

Agilent's Electronic Measurement Group is becoming **Keysight Technologies**.



Engineering Education & Research Resources DVD 2014

Agilent is the key to your test and measurement needs **Order yours**



Strain rate dependence of twinning avalanches at high speed impact

L. Zhang,¹ E. K. H. Salje,^{1,2,a)} X. Ding,^{1,a)} and J. Sun¹

¹State Key Laboratory for Mechanical Behavior of Materials, Xi'an Jiao Tong University, Xian 710049, People's Republic of China

²Department of Earth Sciences, University of Cambridge, Cambridge CB2 3EQ, England

(Received 27 March 2014; accepted 30 March 2014; published online 24 April 2014)

The molecular dynamics simulation of the yield collapse in ferroelastic and martensitic materials under high strain rates shows power law decays of the yield energy. The energy exponent of the “jerk” distribution during yield does not depend on the strain rate and was found to be close to the mean field value of $\varepsilon = 1.35$. The total yield energy changes dramatically during the crossover between the isothermal regime at low strain rates and the adiabatic regime at high strain rates. The crossover point is found in our simulations at 10^{-5} /phonon time which corresponds to strain rates of approximately 10^8 1/s. Faster strain rates occur for high speed impact (shock deformation) with no strain absorption by twinning and no thermal equilibration while slightly slower strain rates lead to rate independent yield energies. © 2014 Author(s). All article content, except where otherwise noted, is licensed under a Creative Commons Attribution 3.0 Unported License.

[<http://dx.doi.org/10.1063/1.4873520>]

When high speed objects hit a martensitic or ferroelastic material, much of its energy is absorbed by the generation of twins and twin boundaries. Applications of this effect range from casings for mobile phones (which should not shatter when they fall on a concrete floor) to shock absorbers and bullet proof vests, and cosmic particles hitting a satellite. In nature, cosmic dust and meteoritic particles also hit moon rocks and minerals on Earth and generates characteristic impact pattern, which often relate to twinning patterns and dislocations. The fundamental physics of this effect is that any mechanical impact will locally increase the density of the target or lead to microstructures such as dislocations, fission tracks, and crack propagation. The impact will also emit shear waves through the material, which can lead to twinning. In this Letter, we describe the second effect: shock induced twinning which has also been observed in sheared Cu.^{1–4} Shock resistance due to martensitic twinning is known in Fe-Mn-Si-Al steels⁵ and is expected in most martensitic and ferroelastic materials.⁶

The atomic scale dynamics of the formation of microstructures during fast impact has not been explored so far. To understand this dynamical process, we consider a simple toy model, which was previously used to explore the dynamics of slow moving twin boundaries and their jamming.⁷ In this model, a martensite is sheared on a local scale. When this shear surpasses the yield point at low strain rates, a multitude of twins will form.^{7–9} This twin pattern is highly complex with a multitude of intersecting twin boundaries, the formation of needle domains and kinks inside twin walls.^{7–9} The dynamics of the formation of the pattern near the yield point is dominated by a high number of energy jerks related to the nucleation and extension of twin patterns. Many of these pattern changes occur in avalanches so that the energy jerks scale the avalanche energies. The yield process was shown previously to follow power law dynamics.^{7–10} The

avalanche dynamics of twinning has been investigated experimentally at low strain rates^{11–13} while little is known for high strain rates. Two questions are tantamount: does the yield process remain scale invariant and if so, does the energy exponent of the power law distribution of the avalanche formation¹⁴ change?

A first attempt to answer these questions was undertaken by Pérez-Reche *et al.*¹⁵ who investigated the effect of thermal driving rates on the avalanche exponents in Cu-Zn-Al and Cu-Al-Ni. Changes by a factor of 100 of the shear rate lead to changes of the exponents by 0.3 in Cu-Zn-Al. Typical rates of the length change of a sample in the laboratory are 3×10^{-3} m/s while the impact of a typical bullet leads to strain rates of 300 m/s. The extrapolated increase of the strain rate by 10^5 would lead to changes of the energy exponent ε of more than 0.6 and should be easy to observe in a computer simulation experiment. We will show, in this Letter, that no such changes are found in our model. Instead, we find that a crossover occurs between low strain rates (with identical absorption energies during yield) and high strain rates where the yield energy becomes explicitly rate dependent. It also implies that fast strain rates do not lead to isothermal equilibration but that the process becomes increasingly adiabatic. A similar crossover at much lower strain rates was previously reported experimentally.¹⁶ We show, in this Letter, that the crossover point coincides with the onset of the collapse of the absorbed energy at the yield point.

We simulate the effect of mechanically driven domain boundaries evolution in two-dimensional (2D) system, using a generic two-body potential to represent the interactions of atoms. The potential energy $U(r)$ is the sum of the first-nearest atomic interactions of $20(r - 1)^2$, the second-nearest interactions $-10(r - \sqrt{2})^2 + 2000(r - \sqrt{2})^4$, and the third-nearest interactions $-(r - 2)^4$, where r is atomic distance. This potential is developed based on Landau theory by choosing the shear angle as “order parameter” and is generic to all ferroelastic materials for studying twinning and

^{a)}Authors to whom correspondence should be addressed. Electronic addresses: ekhard@esc.cam.ac.uk and dingxd@mail.xjtu.edu.cn.



mobility of twin boundaries. The details of properties obtained by this potential are described in our previous work.⁷⁻¹⁰ The equilibrium unit cell is in shape of parallelogram with the shear angle of 4° . We set the equilibrium lattice constant $a = 1 \text{ \AA}$ and atomic mass to $M = 100 \text{ amu}$. The initial condition is a twinned sandwich structure containing two horizontal twin boundaries (HTBs), as shown as point A in Figure 1. The size of 2D simulation box is $500a \times 502a$ ($=50 \text{ nm} \times 50.2 \text{ nm}$), where a ($= 1 \text{ \AA}$) is the lattice repetition unit. The ratio of the height of intermediate layer to the whole sample is fixed to be 0.5. Free boundary conditions are used because we need to consider domain boundaries that nucleate from the free surface. To start our simulations,

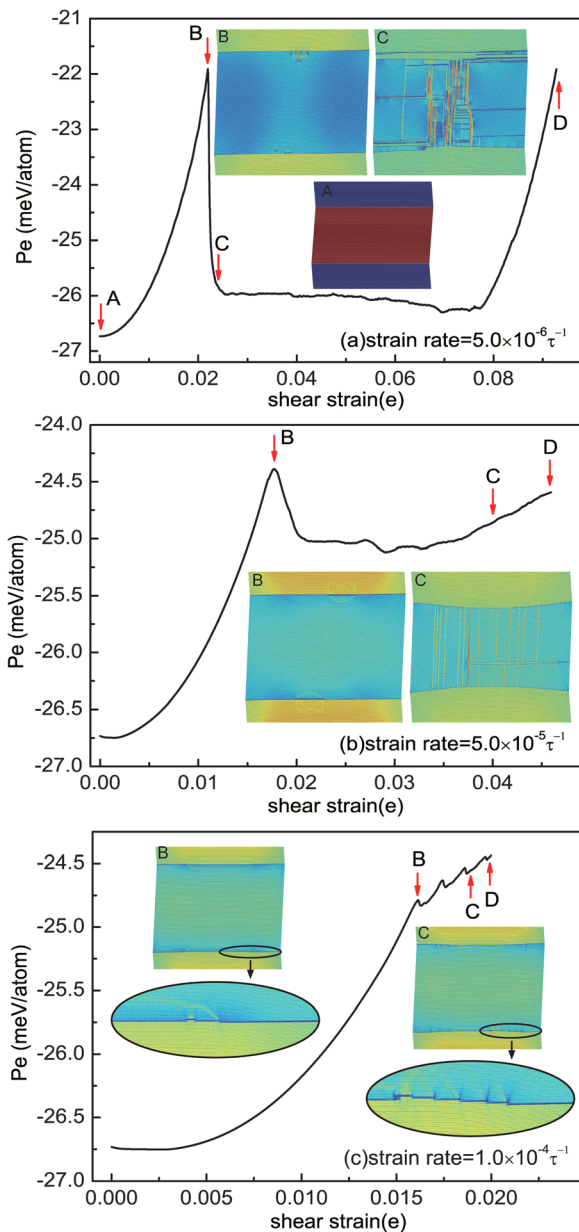


FIG. 1. Evolution of the potential energy Pe with external shear strain e at three different shear strain rates ((a) $5 \times 10^{-6} \tau^{-1}$, (b) $5 \times 10^{-5} \tau^{-1}$, and (c) $10^{-4} \tau^{-1}$). The phonon time is indicated by τ to generalize the model. The inset picture A is the initial model with 2 twin walls. The domain structures at points B and C are shown in the inset pictures B and C. Nucleation of cracks starts at point D and the strain energy is fully released when the crack progresses.

the system was first relaxed with a conjugate gradient refinement procedure to find the optimal position for each lattice point, then molecular dynamics was performed to anneal the configuration at a given temperature for 5×10^6 time steps. The only relaxations that occurred during these procedures were surface relaxations, no further microstructures developed. After relaxation, the top and bottom several layered atoms were then fixed rigidly as the loading grip, and external strains with different strain rates were performed on the twinned structure via a global shear on the two boundary layers. All the calculations are performed using the Large-scale Atomic/Molecular Massively Parallel Simulator, LAMMPS code¹⁷ with an NVT ensemble. We use a low temperature ($T = 0.4 \text{ K}$) and a Nosé-Hoover thermostat^{18,19} to reduce the thermal noise in the simulations. The time scale of our simulations is set by the phonon time. We determined the phonon time in a relaxed sample without external shear and found that 50 MD steps relate to the time τ of one lattice vibration.

The potential energy (Pe) evolution with increasing shear strain (e) is shown for 3 different strain rates (in units of applied strain increment per phonon time) in Fig. 1, the microstructures at the different stages are shown as insets in Fig. 1. We find similar pattern formation for all strain rates with very different amplitudes: the initial state consists of 3 domains with 2 twin walls (point A). Before this sample is sheared to an upper yield point B, the potential energy Pe of the sample in all cases first increases quadratically with increasing external strain. At the upper yield point B, some kinks nucleate in the two twin walls and more complex twin pattern emerge for slow strain rates only (Figs. 1(a) and 1(b)). In this case, the stored potential energy rapidly reduces to the lower yield point C. During this microstructural transformation B-C, a complex twin pattern is formed. Further, increase of the applied strain leads to plastic deformation and de-twinning. However, this is not the case for high strain rate, no yield behavior in the Pe versus e curve is seen (Fig. 1(c)), and only a few kink movement can be found after point B. At the highest strain (point D), we find in all cases the onset and rapid propagation of cracks which destroy the sample.

Fig. 1 also shows that the yield behavior strongly depends on the strain rate. The energy difference between the upper and lower yield points (between points B and C) is the yield energy. The yield energy is largest for low strain rates (Fig. 1(a)), with values similar to results from previous quasi-static simulations.⁷⁻¹⁰ Increasing the strain rate decreases the yield energy from 4 meV/atom at $5 \times 10^{-6} \tau^{-1}$, to 0.5 meV/atom at $5 \times 10^{-5} \tau^{-1}$ (Fig. 1(b)), and to values smaller than 0.01 meV/atom at $10^{-4} \tau^{-1}$ (Fig. 1(c)). The fastest strain rate in our simulations is $10^{-4} \tau^{-1}$. With a phonon time of, say, $\tau = 10^{-13} \text{ s}$, this strain rate is equivalent to 10^9 s^{-1} . The time to acquire a displacement of 100 nm with a typical strain of 1% and a grain size of $10 \mu\text{m}$ would then be equivalent to an impact velocity of 100 m/s. At this strain rate, the yield energy becomes zero and the impact cannot be compensated by pattern formation. The sample becomes hence inert and brittle with no damping mechanism on the time scale of the impact, besides some small kinks nucleating at the performed twin boundaries. After a small increase of strain at this rate, we find nucleation and propagation of cracks (point D in

Fig. 1(c)). Reducing the strain rate to $5 \times 10^{-5} \tau^{-1}$ shows the first sign of a yield behavior where the energy reduces at the upper yield point B and a multitude of vertical twins nucleate (Fig. 1(b)). The complexity of the twin pattern does not change much with decreasing strain rate while the sheared region of the sample increases (Figs. 1(a) and 1(b)). We find, thus, that no shear induced twinning occurs at sufficiently high strain rates while at lower strain rates the domain pattern remains essentially invariant.

The compensation of the impact energy is hence related to the full pattern formation and not due to the nucleation of a few kinks in existing twin boundaries. The collective phenomenon of the twin pattern formation is known to progress via avalanches both for the nucleation and progression of twin boundaries.^{7–10} We analyze the energy evolution of the pattern formation during the shear deformation (Fig. 2) and find energy jerks whenever an avalanche forms. The main activity of jerk formation is in the yield regime while slow strain rates also show jerks in the plastic regime. The same jerks patterns have been observed for much slower strain rates in Ref. 7. We find avalanche behavior whenever a yield point is identifiable (at lower strain rates) and for a strain rate of $5 \times 10^{-5} \tau^{-1}$, also in the plastic regime. An example for a statistical jerk distribution during yield (between points B and C in Figs. 1(b) and 1(c)) is shown in Fig. 3, which indicates that the jerks are power-law distributed. We find that all avalanches follow the same power law statistics as in Fig. 3 with energy exponents near $\varepsilon = 1.35$, within our

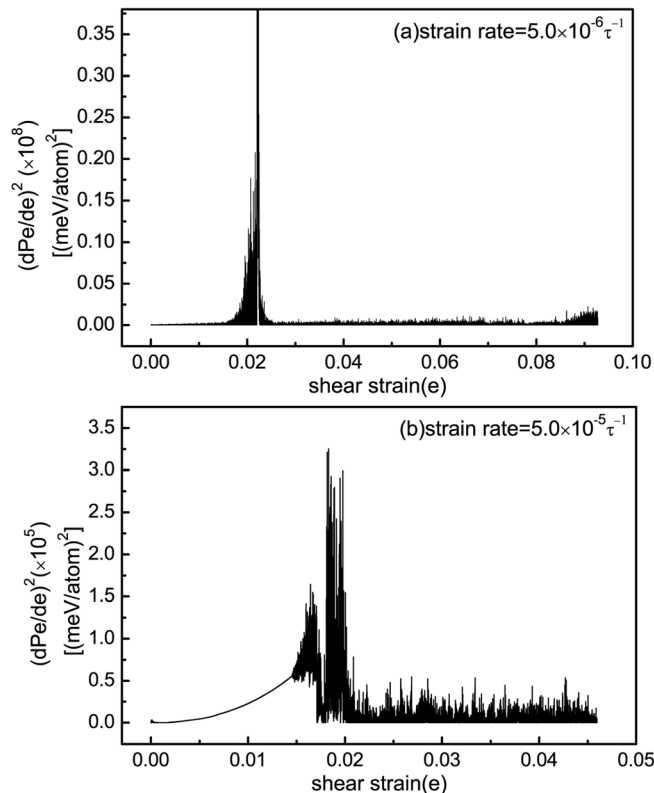


FIG. 2. Noise patterns at slow strain rates (a) $5 \times 10^{-6} \tau^{-1}$ and (b) $5 \times 10^{-5} \tau^{-1}$. The slower strain rate generates avalanches near the yield point. Additional strong avalanches at the strain rate $5 \times 10^{-5} \tau^{-1}$ occur in the plastic regime (between the points C and D in Fig. 1) Precursor yield effects at strains smaller than the yield strain at B are also found for this strain rate.

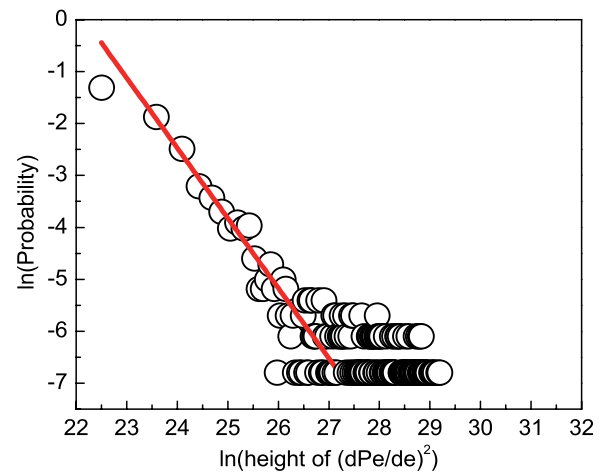


FIG. 3. The jerk spectra during the yield event (between points B and C) at a strain rate of $5 \times 10^{-6} \tau^{-1}$ show a power law distribution $P(E) \sim E^{-\varepsilon}$ with an energy exponent $\varepsilon = 1.35$.

computational resolution, i.e., the energy exponent is the same for all simulations where avalanches could be detected. This value is close to the mean field value¹⁴ for the formation of twin patterns and was also observed experimentally in the martensite alloy $\text{Cu}_{74.08}\text{Al}_{23.13}\text{Be}_{2.79}$ (Ref. 12) and during the collapse of porous SiO_2 -vycor.²⁰ Fig. 4 shows the rate independence of the energy exponent for relatively high strain rates, which is at variance with the results by Pérez-Reche *et al.*¹⁵ who observed changes of a power law exponent at much lower strain rates. We presume that their observed strain rate dependence may be related to the relaxation of external defects and phase mixtures and/or very slow changes of the large twin patterns, which does not exist in our fast impact regime. Such slow relaxations are well known from glasses (α -events) but have not been seen during the propagation of individual twin domains.²¹

The absorbed potential energy at the yield point decays at high strain rates as shown in Fig. 5. For strain rates greater than $10^{-5} \tau^{-1}$, the energy absorption decreases exponentially, and the sample reacts to the impact with high inertia. Simultaneously, the impact increases the sample temperature

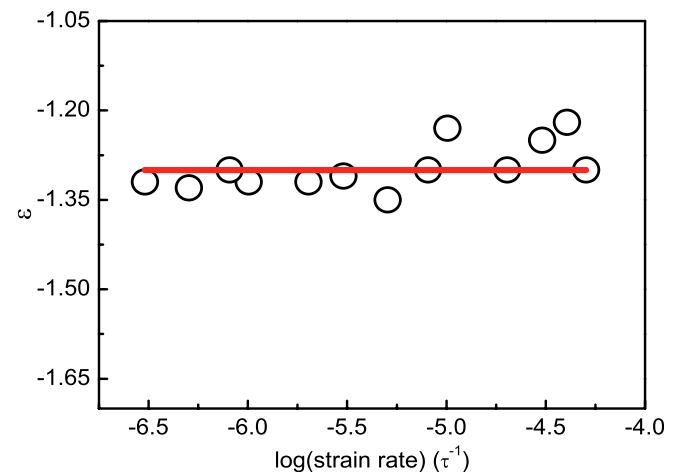


FIG. 4. The change of power law exponent ε during the yield event as function of the strain rate, showing that ε is independent of the strain rate.

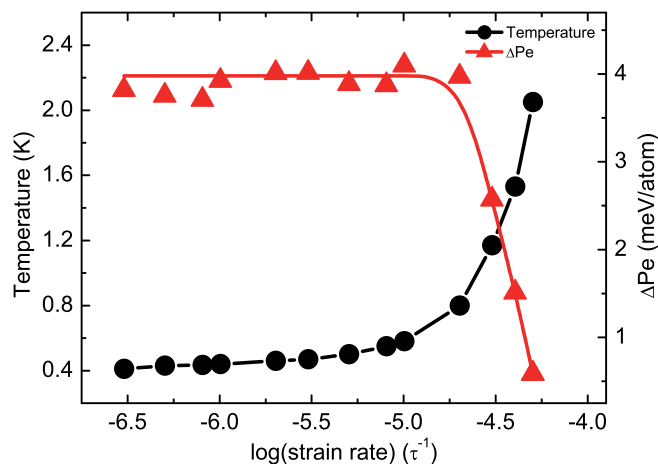


FIG. 5. The change of yield energy ΔPe (energy difference between points B and C) and temperature of the system with different strain rates. ΔPe is constant at low strain rates (isothermal regime) and decays rapidly for strain rates higher than $10^{-5} \tau^{-1}$ (adiabatic regime). The crossover between the isothermal regime and the adiabatic regime is also observed by the heating of the sample at high strain rates.

so that the development of inertia in the pattern formation coincides with the crossover between the isothermal regime at low strain rates and an adiabatic regime at high strain rates. Samples with inertia at high strain rates show cracking (point D in Fig. 1(c)) near the extrapolated yield point so that the sample characteristics change fundamentally from a pliable ferroelastic/martensite to a brittle ceramic.

In summary, we show that the absorption of high-speed impact in martensites and ferroelastic materials is limited to the characteristic strain rate of approximately 10^8 1/s. At lower strain rates, we find the pattern formation to be independent of the strain rate. At higher strain rates, the sample cannot follow the external shear by the formation of twin

boundaries and breaks rather than relaxes into a complex domain pattern.

L.Z., X.D., and J.S. are grateful to NSFC (Nos. 51171140, 51231008, 51321003, and 51320105014) for financial support. EKHS thanks the Leverhulme foundation (RG66640) and EPSRC (RG66344) for financial support.

- ¹F. Cao, I. J. Beyerlein, F. L. Addessio, B. H. Sencer, C. P. Trujillo, E. K. Cerreta, and G. T. Gray III, *Acta Mater.* **58**, 549 (2010).
- ²N. K. Bourne, J. C. F. Millett, and G. T. Gray III, *J. Mater. Sci.* **44**, 3319 (2009).
- ³J. Yang, J. I. Goldstein, E. R. D. Scott, J. R. Michael, P. G. Kotula, T. Pham, and T. J. McCoy, *Meteorit. Planet. Sci.* **46**, 1227 (2011).
- ⁴A. E. Rubin, *Meteorit. Planet. Sci.* **32**, 231 (1997).
- ⁵O. Grässel and G. Frommeyer, *Mater. Sci. Technol.* **14**, 1213 (1998).
- ⁶E. K. H. Salje, *Annu. Rev. Mater. Res.* **42**, 265 (2012).
- ⁷E. K. H. Salje, X. Ding, Z. Zhao, T. Lookman, and A. Saxena, *Phys. Rev. B* **83**, 104109 (2011).
- ⁸X. Ding, Z. Zhao, T. Lookman, A. Saxena, and E. K. H. Salje, *Adv. Mater.* **24**, 5385 (2012).
- ⁹X. Ding, T. Lookman, Z. Zhao, A. Saxena, J. Sun, and E. K. H. Salje, *Phys. Rev. B* **87**, 094109 (2013).
- ¹⁰Z. Zhao, X. Ding, J. Sun, and E. K. H. Salje, *Adv. Mater.* **25**, 3244 (2013).
- ¹¹R. Niemann, J. Baró, O. Heczko, L. Schultz, S. Fähler, E. Vives, L. Mañosa, and A. Planes, *Phys. Rev. B* **86**, 214101 (2012).
- ¹²E. K. H. Salje, J. Koppensteiner, M. Reinecker, W. Schranz, and A. Planes, *Appl. Phys. Lett.* **95**, 231908 (2009).
- ¹³E. Bonnot, E. Vives, L. Mañosa, A. Planes, and R. Romero, *Phys. Rev. B* **78**, 094104 (2008).
- ¹⁴E. K. H. Salje and K. A. Dahmen, *Annu. Rev. Condens. Matter Phys.* **5**, 233 (2014).
- ¹⁵F.-J. Pérez-Reche, B. Tadić, L. Mañosa, A. Planes, and E. Vives, *Phys. Rev. Lett.* **93**, 195701 (2004).
- ¹⁶E. K. H. Salje and W. Schranz, *Z. Kristallogr.* **226**, 1 (2011).
- ¹⁷S. Plimpton, *J. Comput. Phys.* **117**, 1 (1995).
- ¹⁸S. Nosé, *J. Chem. Phys.* **81**, 511 (1984).
- ¹⁹W. G. Hoover, *Phys. Rev. A* **31**, 1695 (1985).
- ²⁰J. Baró, Á. Corral, X. Illa, A. Planes, E. K. H. Salje, W. Schranz, D. E. Soto-Parra, and E. Vives, *Phys. Rev. Lett.* **110**, 088702 (2013).
- ²¹R. J. Harrison and E. K. H. Salje, *Appl. Phys. Lett.* **97**, 021907 (2010).